MATHEMATICAL BIOSCIENCES
AND ENGINEERING
Volume **11**, Number **2**, April **2014**

doi:10.3934/mbe.2014.11.385

pp. **385–401**

COOPERATIVE BEHAVIOR IN A JUMP DIFFUSION MODEL FOR A SIMPLE NETWORK OF SPIKING NEURONS

Roberta Sirovich and Laura Sacerdote

Department of Mathematics "G. Peano", University of Torino
Via Carlo Alberto 10, 10123 Torino, Italy

Alessandro E. P. Villa

Grenoble Institute of Neuroscience Inserm UMRS 836
University Joseph Fourier Grenoble, France
Department of Information Systems, Faculty of Business and Economics
University of Lausanne, CH-1015 Lausanne, Switzerland

Abstract. The distribution of time intervals between successive spikes generated by a neuronal cell –the interspike intervals (ISI)– may reveal interesting features of the underlying dynamics. In this study we analyze the ISI sequence –the spike train– generated by a simple network of neurons whose output activity is modeled by a jump-diffusion process. We prove that, when specific ranges of the involved parameters are chosen, it is possible to observe multimodal ISI distributions which reveal that the modeled network fires with more than one single preferred time interval. Furthermore, the system exhibits resonance behavior, with modulation of the spike timings by the noise intensity. We also show that inhibition helps the signal transmission between the units of the simple network.

1. **Introduction.** In the past fifty years, extensive studies have been dedicated to building good models for single neuron activity. Recently, experimental techniques evolved towards the recording of neuronal activity by means of multiple electrodes which yields the simultaneous and coupled activity of more than one single neuron. From a modeling point of view, these results inspired a shift from single neuronal unit description to the study of networks of neurons.

In this paper we reinterpret a jump diffusion LIF model proposed in [21] in terms of a simple network of spiking neurons. In particular a target neuron A is supposed to receive inputs both from the embedding network of neurons and from two cell assemblies, E and I. The spiking activity of the target neuron A is studied with the objective of understanding the contributions of the different elements which build the system (the background network, E and I) and their interactions. In particular, the following features are discussed:

1. the multimodal shape of the ISI distribution of neuron A;
2. the resonance behavior of the system;
3. the active role of inhibition in signal transmission.

2010 *Mathematics Subject Classification.* 60G99, 60K40, 90B15, 92B20.

Key words and phrases. Noisy leaky integrate and fire, preferred time intervals, stochastic resonance, first exit times, Ornstein Uhlenbeck process, multimodality.

Multimodal ISI histograms may appear in experimental recordings, see for example [5, 17, 31, 11, 18]. It is an interesting point, as each peak of the histogram may be considered a characteristic firing time of the neuron suggesting multiple functional roles of the neuron itself. In the simple network we are considering, each characteristic firing time of the target neuron A, i. e. each mode of its interspike interval distribution, is shown to be the response to different inputs. Despite the overlapping of the information, the neuron discriminates and responds successfully to each source, thus exhibiting different states. From a modeling point of view, multimodality is interesting as well. It has been extensively considered in studies on the response of model neurons to periodic inputs, see [19, 4, 3, 26]. However it can also be observed in experimental data recorded in the absence of any external periodic input. The hereby proposed model is a contribution to this framework, as no periodic input is considered.

The multimodal structure of the ISI histogram recalls the Stochastic Resonance (SR) mechanism, even though it is not itself a signature of SR. Originally, the mechanism of SR was described in bistable nonlinear systems where information is transmitted in the form of hopping events between stable states [20, 30]. Later, several efforts have been devoted to the determination of a SR equivalent in excitable systems with periodic inputs [19, 4, 3]. Other studies investigated the influence of noise on the response of excitable systems to aperiodic (arbitrary) inputs [9, 8, 6]. The role of noise in signal processing and in natural systems is a lasting discussion point [25, 7, 13]. The cooperative behavior of the units of the network described in our model is investigated in this framework and the system is shown to exhibit SR.

Finally, we investigate the role of the inhibitory unit. Inhibition is well known to be regulatory of neuronal excitability. However, despite the limited understanding of the phenomenon, it can be hypothesized that inhibition has also a role in information transmission, see for example [10, 14, 28] and references quoted therein. We propose here a new method to quantify the signal transmission efficiency. Then we use the proposed model to prove that a well tuned inhibition may actually increase the response efficiency of the reference neuron.

The paper is organized as follows: the model and some analytical results are given in Section 2 and in Section 3 the output of the target neuron A is analyzed with regards to the three above presented main topics (multi modality, SR, role of inhibition).

2. **The model.**

A neuron A is supposed to receive inputs from the surrounding network of neurons. The activation of a synapse in the input zone creates a postsynaptic potential (PSP) which is simplified as an instantaneous jump in the modeled membrane potential of the cell A, denoted as V. As the neuron receives over 1,000 presynaptic terminals, its membrane potential, before the occurrence of an action potential, can be described following the well known Stein's model

$$\begin{aligned} dV(t) &= -\frac{V(t)}{\theta}dt + \sum_{j=1}^{n} \alpha_j dP_j^e(t) + \sum_{j=1}^{m} \beta_j dP_j^i(t), \\ V(0) &= 0. \end{aligned}$$

Here $\theta > 0$ is the membrane potential time constant, which accounts for the the spontaneous exponential decay of the membrane potential in the absence of incoming inputs and $\alpha_j > 0$ and $\beta_j < 0$ are the amplitudes of the excitatory and inhibitory PSPs. Each excitatory event reaches neuron A according to a counting

processes P^e (P^i for the evoked inhibitory PSPs) of intensity μ_j^e (μ_j^i respectively). Every postsynaptic potential is below threshold, meaning that PSPs are too small (100 μV to 10 mV, see [15]) to reach the depolarization that activate the voltage–gated ion channels and initiate the action potential. Hence PSPs must summate. Summation of PSPs occurs when presynaptic neurons fire at a sufficiently high rate (temporal summation) or when several presynaptic terminals fire at the same time (spatial summation) or from a combination of temporal and spatial summation. In order to include spatial summation in the model, we simplify the synchronous firing of several presynaptic neurons as one single excitatory or inhibitory input. The assembly of synchronized neuron is represented as a single unit, E for excitatory PSPs and I for inhibitory PSPs, see Fig. 1. Their firing determines strong and sudden changes of amplitudes $e > 0$ (excitatory) and $i < 0$ (inhibitory) in the membrane potential of cell A according to independent counting processes, N^e or N^i. Then the model becomes

$$\begin{aligned} dV(t) &= -\frac{V(t)}{\theta}dt + edN^e(t) + idN^i(t) + \sum_{j=1}^{n}\alpha_j dP_j^e(t) + \sum_{j=1}^{m}\beta_j dP_j^i(t), \\ V(0) &= 0, \end{aligned} \tag{1}$$

which can be read as a generalization of the so called Stein's model, see [27].

The Stein model is not suitable for analytical treatment. For this reason, many approximations have been proposed in the literature, see [16, 23]. Based on these papers, we performed a diffusion limit on the terms accounting for the frequent and small inputs arriving from the surrounding network, i.e. the sums of processes P^e and P^i in (1). Assuming the sizes of the evoked PSPs α_j and β_j going to zero and simultaneously the frequencies μ^e and μ^i going to infinity in such a way that

$$\begin{aligned} \mu &= \lim_{\substack{\mu_j^e,\mu_j^i\to\infty \\ \alpha_j,\beta_j\to 0}} \left(\alpha_j\mu_j^e + \beta_j\mu_j^i\right) \\ \sigma^2 &= \lim_{\substack{\mu_j^e,\mu_j^i\to\infty \\ \alpha_j,\beta_j\to 0}} \left(\alpha_j^2\mu_j^e + \beta_j^2\mu_j^i\right) \end{aligned} \tag{2}$$

we get

$$dV(t) = \left[-\frac{V(t)}{\theta} + \mu\right]dt + \sigma dW(t) + edN^e(t) + idN^i(t), \quad V(0) = 0 \tag{3}$$

where W is a standard Brownian motion, $\mu \in \mathbb{R}$ is the drift and accounts for the mean contribution of all inputs from the embedding network, $\sigma > 0$ is the diffusion term and accounts for the variability of such inputs. It should be noted that an analogous diffusion limit on the terms N^e and N^i in (1) cannot be performed. Indeed these jumps are not infinitesimal and their frequencies prevent a diffusion limit. Eq. (3) describes a jump-diffusion process whose continuous and discontinuous part are respectively the so called Ornstein-Uhlenbeck process and the series of events driven by the two independent counting processes.

The idea of adding inducing–jumps inputs to a continuos diffusion model of the membrane potential is not new and can be found in [21, 24]. However in [21] the biological framework is different as the model was created to account for the geometric structure of the synapses. In particular the main assumption was based on the different weight of distal dendritic synapses and proximal somatic synapses. The latter group was expected to induce larger changes in the membrane potential

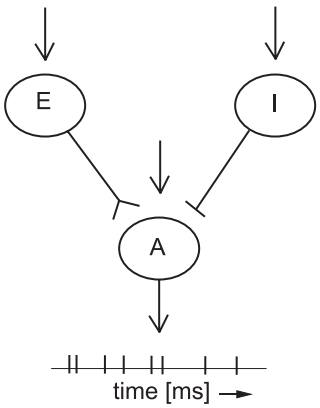

FIGURE 1. A target neuron A embedded in a larger network receives a pool of synchronized inputs from unit E (excitatory) and from unit I (inhibitory).

of the postsynaptic cell as the membrane excitability was assumed to decrease as the distance from the soma increased.

The leaky integrate and fire paradigm is followed to reproduce the spiking mechanism of neuron A and a firing threshold S is introduced: when the membrane potential exceeds for the first time the threshold voltage S the neuron releases a spike. Then the membrane potential is reset to its resting value. We do not assume any feed back mechanism from neuron A to units E and I, so these two units are not reset when A spikes. The sequence of firing times of unit E and unit I, will be a collection of independent and identically distributed times following the interevent distribution of the counting processes N^e and N^i. On the other hand, the sequence of firing times T_j of cell A inherit a dependency structure from the sequence of inputs from E and I.

To properly define the firing times of cell A we introduce the following sequence of stochastic processes. Let us denote as V_1 the process solution of the equation

$$dV_1(t) = \left[-\frac{V_1(t)}{\theta} + \mu\right] dt + \sigma dW(t) + e dN^e(t) + i dN^i(t), \tag{4}$$

with initial condition $V_1(0) = 0$ and implicitly $N^e(0) = N^i(0) = 0$. Then define $T_1 = \inf\{t > 0 : V_1(t) = S\}$ that is the first hitting time of the level S. Next define

$$dV_2(t) = \left[-\frac{V_2(t)}{\theta} + \mu\right] dt + \sigma dW(t + T_1) + e dN^e(t + T_1) + i dN^i(t + T_1), \tag{5}$$

with $V_2(0) = 0$. Note that V_2 inherit the noise term and the counting processes that were driving V_1 but with a random time change. As previously we call $T_2 = \inf\{t > 0 : V_2(t) = S\}$.

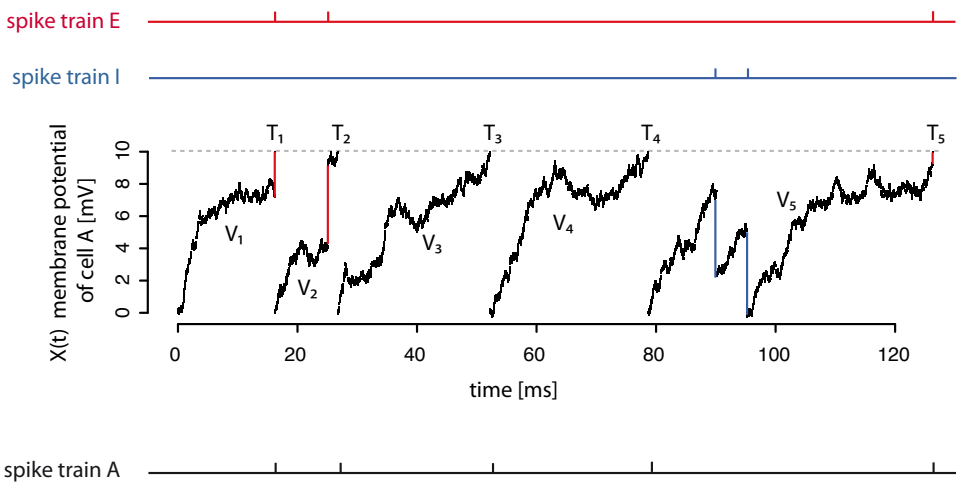

FIGURE 2. Example of a sample trajectory of the membrane potential of cell A given in eq. (7).

For a general $k = 2, 3, \ldots$ we define the sequence of processes

$$dV_k(t) = \left[-\frac{V_k(t)}{\theta} + \mu\right] dt + \sigma dW\left(t + \sum_{j=1}^{k-1} T_j\right) + \\ + e dN^e\left(t + \sum_{j=1}^{k-1} T_j\right) + i dN^i\left(t + \sum_{j=1}^{k-1} T_j\right), \tag{6}$$

with corresponding first passage times $T_k = \inf\{t > 0 : V_k(t) = S\}$. Finally, pasting one after the other the processes V_k, we get the process describing the membrane potential of cell A

$$X(t) = \sum_k V_k\left(t - \sum_{i=1}^{k-1} T_i\right) \mathbf{1}_{(T_{k-1}, T_k]}(t), \tag{7}$$

where $\mathbf{1}_A(x)$ is the indicator function of the set A. An example of trajectory of process (7) is given in Fig. 2.

In particular, in this paper we consider two choices for the counting processes N^e and N^i in (7):

Case 1: two independent counting processes with Inverse Gaussian (IG) distributed intertimes;

Case 2: two independent Poisson processes.

The latter case gives Exponential distributed intertimes and it is a choice motivated by the rare events law which is often suggested in biological literature. In this case, the memoryless property of the Exponential distribution, makes the process (7) a Markov process and despite the absence of a reset of the counting processes P^e and P^i the sequence of firing times of cell A will be a collection of independent and identically distributed random variables. By contrast, the Gaussian distribution is

not memoryless and X in (7) is not a Markov process. Moreover in this case, the sequence of firing times of cell A will not be a collection of independent random variables. The choice of the IG distribution is motivated by the neuronal modeling literature: it is the distribution of the first passage time of a Brownian motion with drift through a constant threshold. Hence with this choice we are modeling units E and I as synchronized perfect integrator model neurons, see [27].

Let us recall that the IG distribution of parameters a and b, IG(a,b), has density

$$f(t;a,b) = \sqrt{\frac{b}{2\pi}} t^{-\frac{3}{2}} \exp\left[-\frac{-b(t-a)^2}{2a^2 t}\right], \quad t>0. \tag{8}$$

In the following sections we will also need the mode (the abscissa of the peak) of this density which is given as

$$m = a\left[\left(1+\frac{9a^2}{4b^2}\right)^{1/2} - \frac{3a}{2b}\right] \tag{9}$$

Through all the manuscript the parameters of the intertime distribution of the excitatory unit E will be denoted as S_e, μ_e and σ_e and analogously for the inhibitory unit I as S_i, μ_i and σ_i. Indeed when $a = |S_e|/\mu_e$ and $b = S_e^2/\sigma_e^2$, eq. (8) gives the distribution of the first passage time of a Brownian motion with drift μ_e and diffusion coefficient σ_e through the boundary S_e.

2.1. **Analytical results on the firing time.** We propose here an approximating equation for the density of the firing time of cell A. Let us remark that the analytical treatment of this problem in the case of counting processes with not Exponentially distributed intertimes is particularly challenging as the resulting membrane potential process is not even markovian. We consider here only the case when the jump processes N^e and N^i in eq. (7) are Poisson processes.

The instantaneous resetting of neuron A after each spike and the Poisson hypothesis on N^e and N^i make the sequence of first passage times $T_k = \inf\{t>0 : V_k(t) = S\}$ of the processes V_k independent and identically distributed. Hence, for the sake of brevity, let us denote the underlying membrane potential jump–diffusion process as V and the first passage time as T. The compound Poisson process obtained as the sum of the processes N^e and N^i is denoted as $N^{e,i}$ and its k–th time of arrival is denoted as $T^{e,i}_{(k)}$.

We are giving a recursive equation for the density of T involving the density of the first passage time of the diffusion process with no jumps (i.e. the Ornstein–Uhlenbeck process, denoted as U). Let us denote as g_x^S the density of the first passage time of the process V originated in x through the threshold S and as d_x^S the corresponding density of the first passage time for the process with no jump component U. Let us consider the following three events

$$\begin{aligned}
\left\{T^{e,i}_{(1)} \geq t\right\} &= \{\text{the first jump occurs after time } t\}\\
\left\{T^{e,i}_{(1)} < t\right\} &= \{\text{the first jump occurs before time } t\}\\
E &= \{\text{the jump is excitatory}\}\\
I &= \{\text{the jump is inhibitory}\}
\end{aligned}$$

and let us consider that

$$\mathbb{P}(T\leq t) = \mathbb{P}(T\leq t|T^{e,i}_{(1)}\geq t)\mathbb{P}(T^{e,i}_{(1)}\geq t) + \mathbb{P}(T\leq t|T^{e,i}_{(1)}< t)\mathbb{P}(T^{e,i}_{(1)}< t).$$

Moreover

$$\begin{aligned}\mathbb{P}(T \le t|T^{e,i}_{(1)} < t) &= \mathbb{P}(T \le t|T^{e,i}_{(1)} < t, E)\mathbb{P}(E|T^{e,i}_{(1)} < t)+\\ &+ \mathbb{P}(T \le t|T^{e,i}_{(1)} < t, I)\mathbb{P}(I|T^{e,i}_{(1)} < t)\\ &= \mathbb{P}(T \le t|T^{e,i}_{(1)} < t, E)\mathbb{P}(E) + \mathbb{P}(T \le t|T^{e,i}_{(1)} < t, I)\mathbb{P}(I)\\ &= \frac{\lambda_e}{\lambda_e+\lambda_i}\mathbb{P}(T \le t|T^{e,i}_{(1)} < t, E) + \frac{\lambda_i}{\lambda_e+\lambda_i}\mathbb{P}(T \le t|T^{e,i}_{(1)} < t, I)\\ &= \frac{\lambda_e}{\lambda_e+\lambda_i}\int_0^t \mathbb{P}(T \le t|T^{e,i}_{(1)} = u, E) f_{T^{e,i}_{(1)}}(u)du+\\ &+ \frac{\lambda_i}{\lambda_e+\lambda_i}\int_0^t \mathbb{P}(T \le t|T^{e,i}_{(1)} = u, I) f_{T^{e,i}_{(1)}}(u)du,\end{aligned}$$

where $f_{T^{e,i}_{(1)}}$ denotes the probability density function of the random variable $T^{e,i}_{(1)}$. Hence going to the density of the first passage time T we have

$$\begin{aligned}g^S_x(t) &= \mathrm{e}^{-(\lambda_e+\lambda_i)t} d^S_x(t) + \lambda_e \int_0^t g^S_{V^S_{u^+}}(t-u)\mathrm{e}^{-(\lambda_e+\lambda_i)u}du+\\ &+ \lambda_i \int_0^t g^S_{V^S_{u^+}}(t-u)\mathrm{e}^{-(\lambda_e+\lambda_i)u}\\ &= \mathrm{e}^{-(\lambda_e+\lambda_i)t} d^S_x(t) + \lambda_e \int_0^t g^S_{U^S_u+e}(t-u)\mathrm{e}^{-(\lambda_e+\lambda_i)u}du+\\ &+ \lambda_i \int_0^t g^S_{U^S_u-i}(t-u)\mathrm{e}^{-(\lambda_e+\lambda_i)u}du \qquad (10)\end{aligned}$$

where the processes V^S and U^S are the processes V and U in the presence of the absorbing threshold S, meaning that $\mathbb{P}(U^S_t \in A) = \mathbb{P}(U_t \in A, T \ge t)$. Let us denote as p_{U^S} its transition probability functions. Then we have

$$\begin{aligned}g^S_x(t) &= \mathrm{e}^{-(\lambda_e+\lambda_i)t} d^S_x(t)+\\ &+ \lambda_e \int_0^t \left(\int_{-\infty}^{S-e} g^S_{z+e}(t-u) p_{U^S}(z,u|x)dz+\right.\\ &+ \left.\int_{S-e}^{S} p_{U^S}(z,u|x)\delta(u-t)dz\right)\mathrm{e}^{-(\lambda_e+\lambda_i)u}du+\\ &+ \lambda_i \int_0^t \left(\int_{-\infty}^{S} p_{U^S}(z,u|x,0) g^S_{z-i}(t-u)dz\right)\mathrm{e}^{-(\lambda_e+\lambda_i)u}du. \qquad (11)\end{aligned}$$

Eq. (11) can be used recursively to get an approximation of the first passage time density g^S_x. All the terms in the r.h.s. of the equation are known. Indeed the density d^S_x of the first passage time of the process U, i.e. the process with no jumps which is an Ornstein Uhlenbeck process, can be calculated using one of the methods reviewed in [1]. Moreover, the transition density of the Ornstein Uhlenbeck process U in the presence of the absorbing threshold can be evaluated as

$$p_{U^S}(x,t|y,s) = p_U(x,t|y,s) - \int_s^t g^S_y(\tau) p_U(x,t|S,\tau)d\tau. \qquad (12)$$

However let us remark that the computations required to get a good approximation are quite demanding. For this reason we decided to rely on Monte Carlo simulations

even in the case of Poissonian jumps where actually a numerical approximation can be achieved by means of eq. eq. (11).

3. **Results.** We hereby focus on some qualitative features of the spiking activity of cell A, in order to determine:

- the role of the parameters involved in the proposed neuronal model;
- the rise of complex dynamics determined by the coupling of synchronized inputs (from E and I) to the "background" activity of the network;
- the role of inhibition in signal transmission.

When N^e and N^i are two independent counting processes with IG distributed intertimes, no closed form expression is available for the distribution of the interspike times T_i. Moreover the numerical approximation in the Poissonian case (11) is quite complicated to implement. Hence, for the examples of this Section we used computer simulations. The simulation algorithm is a generalization of the exact generation of trajectories of an Ornstein Uhlenbeck process by means of the transition density in order to include the jumps events. The first passage time is deduced from the trajectories evaluating possible hidden crossings in between the nodes of the time discretization, as suggested in [12, 2].

We selected the values of the parameters into biological ranges but we did not test a specific physiological case as our aim was rather to study the qualitative features of the neuromimetic model. The only parameters that are kept constant through all the paper are the threshold level $S = 10$ mV and the resetting potential $V(0) = 0$ mV. We choose to limit our examples to the case of balanced activity of the units E and I motivated by two reasons:

- we tested the model with unbalanced inputs from E and I and we have not observed special interesting features;
- the balanced setting gives a zero mean signal from E and I which cannot hide the activity of the surrounding network.

Few words should be spent about the parameters e and i that result from the spatial summation of several excitatory and inhibitory PSPs generated at the same time. We consider $e = -i = 5$ mV. Even if their role in the model lead to choose "large" values for such parameters and 5 mV could be plausible, see [15], our choice is hardly motivated by the physiological knowledge. Indeed on the basis of the physiological knowledge we should prefer smaller amplitudes, at most around 2-3 mV. However, once we checked that the results were qualitatively unchanged, we moved to extreme values as 5 mV in order to intensify the features of the spiking activity of cell A that are the object of the next Sections and to speed up the computational time of the simulations. In particular, the multimodality of the ISIs distribution of cell A, which is the core of this manuscript, is shown to be robust to changes of the amplitude of the positive and negative jumps, e and i, see Fig. 3–panels **a1**–**a4**.

Simulation batches are performed with samples of $N = 10,000$ spikes of the target neuron A. At each run the spike trains of units A, E and I (i.e., the epochs of the events) are recorded and the ISIs are calculated.

3.1. **Multimodal interspike interval distribution.** It is remarkable that the ISIs distribution of the neuron A is multimodal, see Figures 3–4. We observed shapes similar to those in Figures 3–4 for a wide range of values of the parameters even if though in our study there is no oscillatory term (we will investigate the nature of the signal from E and I in Section 3.2).

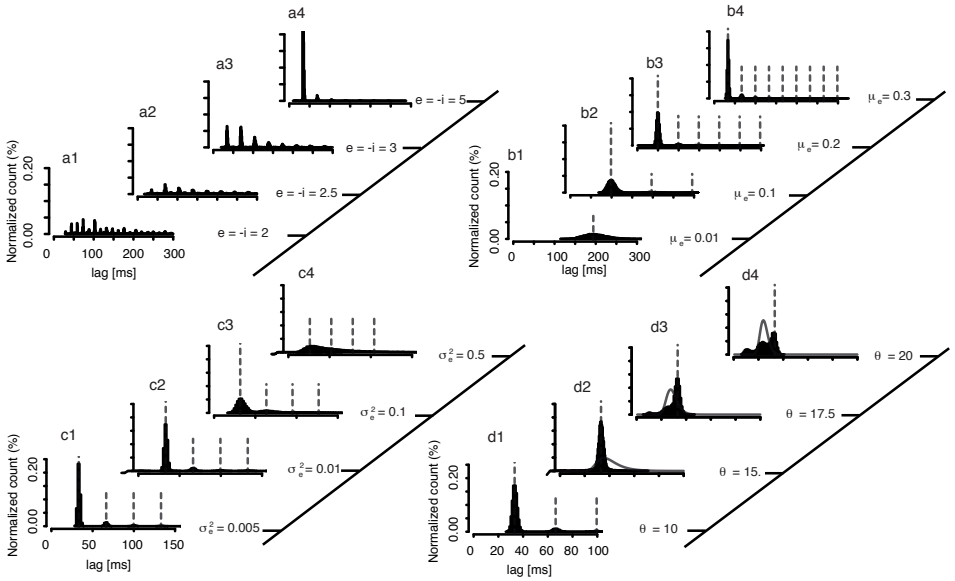

FIGURE 3. Neuron A with IG modeled units E and I: ISI histograms. Common parameters: $S = 10$ mV, $\mu = 0.7$ mV, $\sigma^2 = 0.05$ mV^{2}ms^{-1}, $S_e = S_i = 10$ mV. **Panels a1–a4**: $\theta = 10$ ms, $\mu_e = \mu_i = 0.3$ mVms^{-1}, $\sigma_e^2 = \sigma_i^2 = 0.01$ mV^{2}ms^{-1}. The values of the varying parameter are: $e = 2$ (**a1**), $e = 2.5$ (**a2**), $e = 3$ (**a3**) and $e = 5$ (**a4**). **Panels b1–b4**: $\theta = 10$ ms, $\sigma_e^2 = 0.01$ mV^{2}ms^{-1} and $e = -i = 5$ mV. The values of the varying parameter are: $\mu_e = 0.3$ (**b4**), $\mu_e = 0.2$ (**b3**), $\mu_e = 0.1$ (**b2**) and $\mu_e = 0.01$ (**b1**). The vertical dotted lines correspond to the values $t_k = k \cdot 33.17$ (**b1**), $t_k = k \cdot 49.63$ (**b2**), $t_k = k \cdot 98.51$ (**b3**), $t_k = k \cdot 194.09$ (panel **b4**) obtained from eq. (9). **Panels c1–c4**: $\theta = 10$ ms, $\mu_e = \mu_i = 0.3$ mVms^{-1} and $e = -i = 5$ mV. The values of the varying parameters are: $\sigma_e^2 = 0.005$ (**c1**), $\sigma_e^2 = 0.01$ (**c2**), $\sigma_e^2 = 0.1$ (**c3**) and $\sigma_e^2 = 0.5$ (**c4**). The vertical dotted lines correspond to the values $t_k = k \cdot 33.17$ obtained from eq. (9). **Panels d1–d4**: $\mu_e = \mu_i = 0.3$ mVms^{-1}, $\sigma_e^2 = \sigma_i^2 = 0.01$ mV^{2}ms^{-1} and $e = -i = 5$ mV. The values of the varying parameter are: $\theta = 10$ (**d1**), $\theta = 15$ (**d2**), $\theta = 17.5$ (**d3**) and $\theta = 20$ (**d4**). The vertical dotted lines correspond to the values $t_k = k \cdot 33.17$ obtained from eq. (9). The continuous line in each panel is the corresponding density of the firing time of a neuron modeled as an Ornstein Uhlenbeck process, eq. (7) with $e = i = 0$.

Each peak of the histograms in Figures 3–4 corresponds to a characteristic firing time of the neuron. In order to understand the causes of these peaks we will discuss a set of examples and two cases will be distinguished for activity modeling of units E and I: counting processes generated by IG case and the Poisson case.

Let us enter a detailed study.

Case 1: N^e and N^i with IG distributed intertimes. The parameters can be separated in two families:

1. the parameters regulating the activity of units E and I, i. e. S_e, μ_e, σ_e and S_i, μ_i, σ_i
2. the parameters linked to the embedding network, S, μ, θ and σ

We herein present results based on the dependency on the first family of parameters and on the second family of parameters in Figure 3.

From a first look at the Figure, we see several peaks in the histograms. They can be very regularly spaced and separated, see Fig. 3 panels **a1**–**a4**, **b3, b4**, **c1**–**c3**, and panel **d1**, but also partially overlapped and irregular, see Fig. 3 panels **d3, d4**.

The abscissae of the peaks are determined by the frequency of the evoked excitatory PSPs from unit E. Indeed, named m the mode of the IG distribution in eq. (9), the peaks appear at times $t_k = k \cdot m$, for $k \in \mathbb{N}$. With the parameters of Fig. 3–panels **b1**–**b4** we predict peaks at positions $t_k = k \cdot 33.17$ panel **b4**, $t_k = k \cdot 49.63$ panel **b3**, $t_k = k \cdot 98.51$ panel **b2**, $t_k = k \cdot 194.09$ panel **b1**, as indicated by the vertical dotted gray lines. The parameter σ_e has a double role: it determines both the position of the peaks and their width. Larger values of σ_e increase the variability of the activity of unit E determining wider peaks. When σ_e is large, the peaks completely mix up in a single scattered peak, see Fig. 3 panel **c4**. In panels **b1**–**c4**, the discontinuous part dominates the dynamics, due to the choice of the parameters involved in the diffusive part of model (7), μ, θ and σ. This fact facilitates the analysis of the role of units E and I in the figures. Nevertheless, the contribution of the embedding network is critical. In the absence of the diffusion component, cell A has unimodal ISI distribution with abscissa of the maximum at time $t_2 = 2 \cdot m$. Indeed, two jumps of amplitude $e = 5$ mV determined by unit E are necessary to cross the threshold $S = 10$ mV.

In panels **d1**–**d4** the parameter θ is changed. The Figure illustrate two different regimes of the ISI distribution of the target neuron A. In the first case, the peaks are very regularly spaced and clearly separated (see panel **d1**). In the second case, the peaks are partially overlapped and irregular (see panels **d3**–**d4**). Furthermore, in these last panels, a first peak appears at $t_1 < m$. In the transition from the first regime to the second one (see panel **d2**), the distribution becomes nearly unimodal. Completely similar results can be obtained studying the dependency on μ, but the corresponding Figure is omitted for the sake of brevity.

These observations suggest the existence of two different dynamics of neuron A in correspondence to two domains in the space of the parameters θ and μ:

1. *subthreshold* regime: $\mu \cdot \theta < S$ (cell A behaves according to the first regime);
2. *suprathreshold* regime $\mu \cdot \theta > S$ (cell A behaves according to the second regime).

In the *subthreshold* regime, the process (7), crosses the constant boundary S exclusively due to the presence of the noise of intensity σ. The coupling of the dynamics determined by the continuous and by the discrete parts of the model (7) is dominated by the activity of units E and I. Conversely, in the *suprathreshold* regime, two phenomena concur to the crossing of the threshold: the deterministic trend associated with the drift term μ and the synchronous activity of excitatory unit E.

The features of the output of neuron A are determined by the superimposition of three sources of "signal" in the system: the network, unit E and unit I. Fig. 3 panels **d1**–**d4** shows that neuron A is able to decompose these three input signals.

The different panels illustrate the output of neuron A as the continuous component of process (7) becomes stronger. The gray continuos line in panels **d4** is the first passage time through the threshold S determined by the signal from the surrounding network in the absence of activity of the units E and I. Its shape shifts towards shorter times and reduces its variability as θ increases. When the units E and I are active, the ISIs histogram exhibits a peak at the same epoch as the histogram determined by a pure diffusive input. The other peak at time $t_1 = m$, is driven by the excitatory unit E. It looses mass as the diffusion input increases with θ. Finally we observe a very early peak around time $t_0 \sim 10$, driven by the interaction of the three sources of activity which gains mass as θ increases.

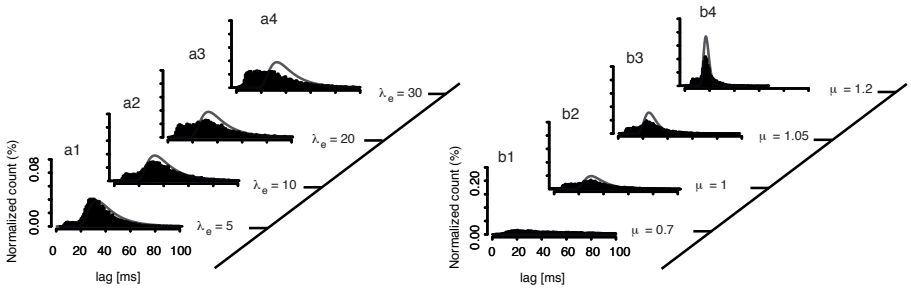

FIGURE 4. Neuron A with Poisson units E and I: ISI histograms. Common parameters: $S = 10$ mV, $\theta = 10$ ms, $\sigma^2 = 0.05$ mV^{2}ms^{-1}, $e = -i = 5$ mV. **Panels a1–a4**: $\mu = 1$ mVms^{-1} and $\lambda_e = 5$ (**a1**), $\lambda_e = 10$ (**a2**), $\lambda_e = 20$ (**a3**) and $\lambda_e = 30$ (**a4**) ev/s. **Panels b1–b4**: $\lambda_e = \lambda_i = 20$ ev/s and $\mu = 0.7$ (**b1**), $\mu = 1$ (**b2**), $\mu = 1.05$ (**b3**) and $\mu = 1.2$ (**b4**) mVms^{-1}. The continuous line in each panel is the corresponding density of the firing time of a neuron modeled as an Ornstein Uhlenbeck process, eq. (7) with $e = i = 0$.

Case 2: N^e and N^i Poisson processes. In Figure 4 we illustrate the case with excitatory and inhibitory inputs from units E and I which arrive according to Poisson counting processes, i.e. Exponential interarrival times.

The ISIs of unit A are mainly bimodal. Furthermore, the regimen with many well distinguished peaks are not exhibited in the presence of Poisson inputs. When the diffusive part of the process (7) is in the strongly *subthreshold* regime(see panel **b1**), the firing distribution is over dispersed. This feature is typical of the Poisson process and it is the result of the superimposition of the Poissonian activity of the two units E and I and of an analogous Poissonian behavior of the embedding network. Indeed, in the *subthreshold* regimen, even the output determined by the surrounding network is Poissonian, see [29, 22].

Bimodal histograms result from the coupling between the synchronous activity of unit E and I and the network. As μ increases, the output determined by the surrounding network is no more Poissonian and the distribution splits up in two peaks, see panels **b2–b4**. One is placed at the lags corresponding to the peak of the distribution of the firing time when units E and I are silent (cf. continuous

line). The other one appears at shorter times, hence it anticipates the firing with respect to the response to the network activity.

The strong connection between bimodality in firing times and response to superimposed synchronous and diffusive inputs is confirmed in panels **a1**–**a4**. When λ_e and λ_i strongly increase, the synchronous inputs dominate and the histograms become unimodal (panel **a4**). The same happens when λ_e and λ_i are small enough and the inputs from the surrounding network dominate (panel **a1**).

3.2. **Resonance behavior: The role of noise.** To enter the classical SR paradigm, the "signal" and the "noise" component of the system should be properly identified. In the model here studied, the "noise" component can be easily recognized as the continuous part of eq. (7), which is given by an Ornstein Uhlenbeck process. On the other hand, the "signal" is the discontinuous part, namely the jumps occurring when the units E and I release synchronous spikes. Hence, it seems as if no periodic component was present in the "signal". However, the case where synchronized units fire with IG distributed intertimes could be considered at least "almost–periodic". This fact becomes evident if we pass a unit–area symmetric Hanning window filter over the time series of the pulses corresponding to the spike events from units E and I (the so called spike train). In Fig. 5 we illustrate the filtered spike trains from E (panel **a** IG and panel **d** Exponential intertimes), from I (panel **b** IG and panel **e** Exponential intertimes) and the sum of them (panel **c** IG and panel **f** Exponential intertimes). In the IG case, the filtered signal, obtained by

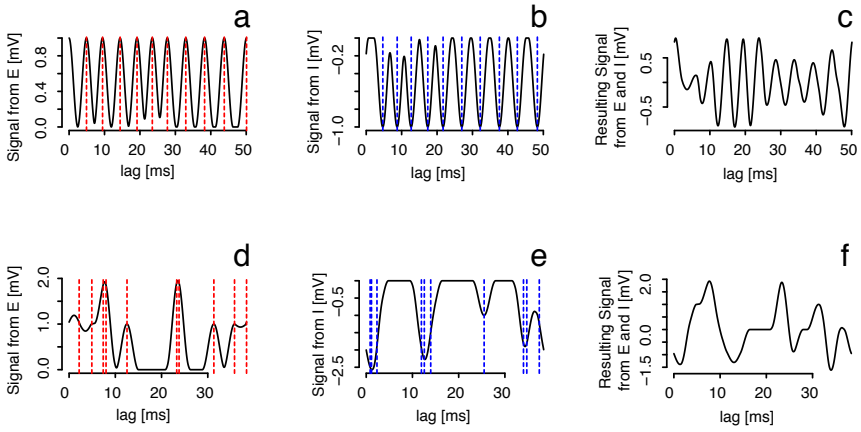

FIGURE 5. Examples of signals from E and I filtered by a symmetric Hanning window of 5 ms. IG modeled units E and I (panels **a**–**c**) and Poisson modeled units E and I (panels **d**–**f**). In **a**, filtered signal from a spike train made of 10 excitatory events (vertical dotted red lines) for $S_e = 10$ mV, $\mu_e = 0.2$ mVms^{-1}, $\sigma_e^2 = 0.5$ mV^{2}ms^{-1}. In **b**, filtered signal from a spike train made of 10 inhibitory events (vertical dotted blue lines) with the same parameters as in **a**. In **c**, filtered signal from the sum of the spike trains in **a** and **b**. In panels **d**–**f** the corresponding examples for the Poisson model with $\lambda_e = \lambda_i = 20$ ev/s.

the superimposition of the excitatory and inhibitory synchronized inputs in panel

c, shows some weakly periodic behavior. Indeed, this signal looks like a sine wave with variable amplitude, whose characteristics depend on the alternance between positive and negative inputs. Its period is affected by random small drift resulting from the small random perturbation of the intertimes between firing events. As it can be asserted, the dominant frequency is equal to $1/m$, where m is the mode of the IG distribution given in eq. (9).

If we filter the spike trains from units E and I with Exponential distributed intertimes we find a completely different resulting signal, see Fig. 5 panels **d**–**f**. This is related to the memoryless property of the Exponential distribution. As this feature is exclusive of the Exponential distribution, the resulting signal will have a non–predictable shape only for Exponential intertimes. By contrast, it will appear weakly periodic for any other distribution of intertimes provided that variance is not too large.

As a consequence of these remarks, we decided to investigate the cooperative behavior between the "signal" (evoked PSPs due to the activity of units E and I) and the "noise" (from the embedding network of neurons) only for IG distributed intertimes in the signal component of the system. We choose between a set of parameters coherent with the investigations in the usual SR framework and weak "signal" was considered a condition in which the cell fires with very low probability (but not zero), in the absence of "noise". Furthermore our analysis is limited to choices of the parameter compatible with the *subthreshold* regime.

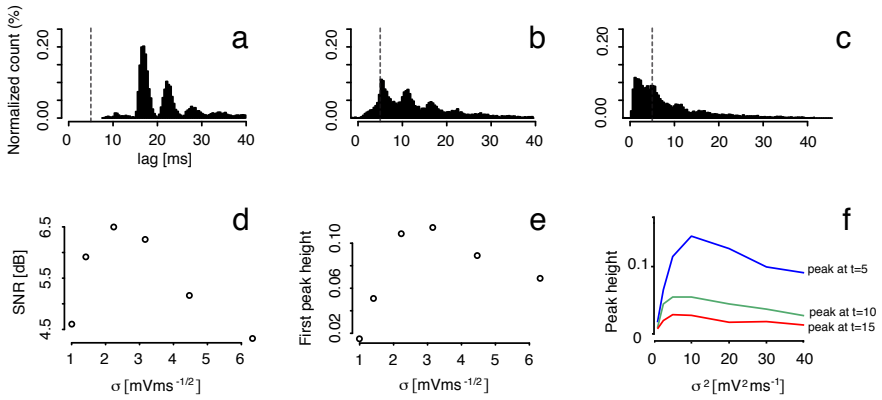

FIGURE 6. Histograms of the ISI of the target neuron A with IG modeled units E and I. Here $\sigma^2 = 10^{-3}, 5, 10$ mV^{2}ms^{-1} (panels **a**, **b**, **c**) and $S = S_e = 10$ mV, $\theta = 10$ ms, $\mu = 0.9$ mVms^{-1}, $\mu_e = 2$ mVms^{-1}, $\sigma_e^2 = 0.5$ mV^{2}ms^{-1}, $e = i = 5$ mV. In **d**, signal to noise ratio (SNR) as a function of σ. In **e**, height of the peak at lag $t = 5$ as a function of σ. In **f**, height of the peaks at lags $t_1 = 5$, $t_2 = 10$ and $t_3 = 15$ for the following choice of the parameters: $\mu = 0$ mVms^{-1}, $\theta = 9$ ms, $e = -i = 7$ mV.

The most common way to quantify SR is through the signal–to–noise ratio (SNR), given as the ratio between the strength of the peak located at the signal frequency in the power spectrum of the spike train and the background noise level. In particular it can be calculated as $10 \log_{10}(S/N)$ dB, where S is the area enclosed above the noise

background and N is the amplitude of the noise background at the signal frequency. Evidence of SR is a maximum in the SNR at an optimal value of noise intensity. Alternatively SR can be identified through the analysis of the ISI distribution. In particular the heights of individual peaks should go through maxima for critical values of the noise strength, here represented by the diffusion parameter σ^2.

In Fig. 6 the results of the investigation are illustrated for both the measures of SR, the SNR (panel **d**) and the ISI distribution (panels **e**–**f**). In both cases SR can be determined. The SNR and the height of the first peak (located at the dominant frequency $1/m$) goes through a maximum as a function of the noise intensity. Conversely, the second, third and fourth peaks show a monotonically decreasing height. Let us deepen the comprehension of the different behavior of the heights of the peak in the ISI histogram. The peak located at lag $1/m$ is made up of noise induced firing times of cell A. Hence the noisy crossing of the threshold gradually synchronizes with the signal, which is exactly the paradigm of SR. The next peaks are no more noise induced, as can be deduced from the ISI in Fig. 6 panel **a**. Though the noise intensity is very small, $\sigma^2 = 10^{-3}$ $\mathrm{mV^2ms^{-1}}$, the peaks are clearly observable. They are determined by the synchronization of the signal with the threshold crossings. This synchronism is caused by the drift term μ. Indeed the drift leads the membrane potential to large enough values which allows the cell to fire when an excitatory PSP is evoked. Hence those peaks do not show resonance behavior because they are actually not related to the cooperation between signal and noise in the system. To strengthen this argument let us notice that if the drift term μ is removed from eq. (7) ($\mu = 0$) it can be proved that all the peaks in the ISI distribution show a maximum as a function of the noise intensity, see Fig. 6 panel **f**.

3.3. **The role of inhibition in signal transmission.** In this section we investigate the role of the inhibitory unit I in the signal transmission. As the role of the excitatory unit E can be clearly deduced from the above–mentioned results, the role of inhibition may be not so obvious. In order to investigate this subject let us quantify the part of the signal that we consider successfully transmitted by the neuron A.

The flow of information transmitted throughout a system can be measured as a coherence between the input stimulus and the system response. In our problem, the input stimulus and the system response are respectively represented by the excitatory PSPs from unit E and the output spikes from the target neuron A. Both stimulus and response are modeled as point events. We propose to measure the coherence between stimulus and response as the fraction of events in the spike train produced by neuron A which are caused by an excitatory event in the spike train produced by unit E. This is the portion of events in the A spike train which are synchronous to an event in the E spike train. We call such a proportion *response efficiency* (RE) and it is given as

$$\mathrm{RE} = \frac{\#\{T_j : |T_j - T_k^e| < \mathrm{tol}\}}{\#\{T_j\}}, \tag{13}$$

where T_j are the ISIs in the A spike train, T_k^e are the ISIs in the E spike train and 'tol' is a fixed tolerance for calling synchronous two events that differ less than 'tol'.

Let us calculate the RE of the system both in the presence and in the absence of inhibitory activity from unit I. The results are reported in Fig. 7. The left panel considers the case with IG distributed intertimes, while the right panel considers

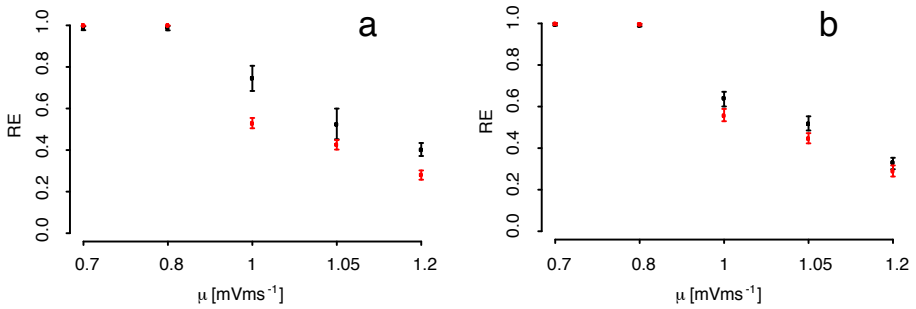

FIGURE 7. Monte Carlo confidence intervals at the level 95% for the response efficiency (RE) defined in eq. (13) for different values of μ. Left panel, IG modeled units E and I. Right panel, Poisson modeled units E and I. Here $S = S_e = 10$ mV, $\theta = 10$ ms, $\sigma^2 = 0.05$ mV^{2}ms^{-1}, $\mu_e = 0.3$ mVms^{-1}, $\sigma_e^2 = 0.01$ mV^{2}ms^{-1}, tol$= 0.1$ ms. Black lines $e = -i = 5$ mV, red lines $e = -i = 0$ mV.

the Poissonian case. The figure contains the plots of the 95% level Monte Carlo confidence interval calculated on a sample of size 100 made up of sample RE, each of them obtained from a spike train with 1000 firing events of cell A. The samples have been simulated for different values of μ, both in the presence (black lines) and in the absence (red lines) of inhibitory activity from I. From a first look at the figure we can assert that the RE for the IG and the Poisson case exhibits analogous behaviors. If the role of inhibition is considered, as the process moves from *subthreshold* to *suprathreshold* regime, the RE levels show different behaviors of the network. When the diffusion term is in the *subthreshold* regime, the signal from the network embedding cell A is not strong enough to induce a response. As the chosen noise level is very small ($\sigma^2 = 0.05$ mV^{2}ms^{-1}), the firing activity of cell A is fully driven by the excitatory unit. This is supported in Fig. 7 by the confidence intervals for $\mu = 0.7$ and $\mu = 0.8$ mVms^{-1} that are located near to value 1, meaning that almost all spikes from A are synchronous to a spike from E. In the *suprathreshold* regime, the network signal is stronger and may produce a response of cell A. Hence its firing activity will be competitively driven both from E and the network. Consequently, the RE assumes lower values even if the signal from E has the same strength. In this regime the role of inhibition can be appreciated. Indeed, in the presence of inhibition (black confidence intervals) cell A responds with higher efficiency to the synchronous excitatory inputs from E (larger values of RE) if compared to the response in the system with no inhibition (red confidence intervals). This suggests an active role of inhibition in the synchronization of neural firing and in information processing.

4. **Conclusions.** We propose a jump diffusion LIF model for a neuron belonging to a network in spontaneous activity and receiving inputs from two independent units of synchronous neurons. This formal neuron is able to distinguish different inputs. Its output ISIs distribution is multimodal and each peak is determined by a specific input. Furthermore we observe a stochastic resonance behavior and we relate it with the synchronous inputs from the excitatory unit. A further feature of

the proposed model concerns the role of inhibition. Indeed we show that inhibition increases the information transmission efficiency of the neuron. Future studies could consider a larger variety of activity from sets of synchronous units.

Acknowledgments. We would like to thank the referees for their valuable comments and suggestions. Work partially supported by the University of Torino on the 2012 research project "Stochastic Processes and Applications".

REFERENCES

[1] L. Alili, P. Patie and J. L. Pedersen, Representations of the first hitting time density of an Ornstein-Uhlenbeck process, *Stoch. Models*, **21** (2005), 967–980.
[2] P. Baldi and L. Caramellino, Asymptotics of hitting probabilities for general one-dimensional pinned diffusions, *Ann. Appl. Probab.*, **12** (2002), 1071–1095.
[3] A. R. Bulsara, T. C. Elston, C. R. Doering, S. B. Lowen and K. Lindenberg, Cooperative behavior in periodically driven noisy integrate-fire models of neuronal dynamics, *Phys. Rev. E*, **53** (1996), 3958–3969.
[4] A. R. Bulsara, S. B. Lowen and C. D. Rees, Cooperative behavior in the periodically modulated Wiener process: Noise-induced complexity in a model neutron, *Phys. Rev. E*, **49** (1994), 4989–5000.
[5] W. H. Calvin and C. F. Stevens, Synaptic noise and other sources of randomness in motoneuron interspike intervals, *J. Neurophysiol.*, **31** (1968), 574–587.
[6] A. Capurro, K. Pakdaman, T. Nomura and S. Sato, Aperiodic stochastic resonance with correlated noise, *Phys. Rev. E*, **58** (1998), 4820–4827.
[7] G. A. Cecchi, M. Sigman, J.-M. Alonso, L. Martínez, D. R. Chialvo and M. O. Magnasco, Noise in neurons is message dependent, *Proceedings of the National Academy of Sciences*, **97** (2000), 5557–5561.
[8] J. J. Collins, C. C. Chow, A. C. Capela and T. T. Imhoff, Aperiodic stochastic resonance, *Phys. Rev. E*, **54** (1996), 5575–5584.
[9] J. J. Collins, C. C. Chow and T. T. Imhoff, Aperiodic stochastic resonance in excitable systems, *Phys. Rev. E*, **52** (1995), R3321–R3324.
[10] I. Duguid, T. Branco, M. London, P. Chadderton and M. Häusser, Tonic inhibition enhances fidelity of sensory information transmission in the cerebellar cortex, *The Journal of Neuroscience*, **32** (2012), 11132–11143.
[11] M. Gernert, M. Bennay, M. Fedrowitz, J. H. Rehders and A. Richter, Altered discharge pattern of basal ganglia output neurons in an animal model of idiopathic dystonia, *J. Neurosci.*, **22** (2002), 7244–7253.
[12] M. T. Giraudo and L. Sacerdote, An improved technique for the simulation of first passage times for diffusion processes, *Comm. Statist. Simulation Comput.*, **28** (1999), 1135–1163.
[13] L. L. Gollo, C. R. Mirasso and A. E. P. Villa, Dynamic control for synchronization of separated cortical areas through thalamic relay, *NeuroImage*, **52** (2010), 947–955.
[14] M. Häusser and B. A. Clark, Tonic synaptic inhibition modulates neuronal output pattern and spatiotemporal synaptic integration, *Neuron*, **19** (1997), 665–678.
[15] E. R. Kandel, J. H. Schwartz and T. M. Jessell, *Principles of Neural Science*, Vol. 4, McGraw-Hill, New York, 2000.
[16] P. Lánský, On approximations of Stein's neuronal model, *J. Theor. Biol.*, **107** (1984), 631–647.
[17] M. W. Levine and J. M. Shefner, A model for the variability of interspike intervals during sustained firing of a retinal neuron, *Biophysical Journal*, **19** (1977), 241–252.
[18] Y. Loewenstein, S. Mahon, P. Chadderton, K. Kitamura, H. Sompolinsky, Y. Yarom and M. Häusser, Bistability of cerebellar Purkinje cells modulated by sensory stimulation, *Nature Neuroscience*, **8** (2005), 202–211.
[19] A. Longtin, Stochastic resonance in neuron models, *Journal of Statistical Physics*, **70** (1993), 309–327.
[20] A. Longtin, A. Bulsara and F. Moss, Time interval sequences in the bistable systems and the noise-induced transmission of information by sensory neurons, *Phys. Rev. Lett.*, **67** (1991), 656–659.

[21] M. Musila and P. Lánský, Generalized Stein's model for anatomically complex neurons, *Biosystems*, **25** (1991), 179–191.
[22] A. G. Nobile, L. M. Ricciardi and L. Sacerdote, Exponential trends of Ornstein-Uhlenbeck first-passage-time densities, *J. Appl. Probab.*, **22** (1985), 360–369.
[23] L. M. Ricciardi, Diffusion approximation for a multi-input model neuron, *Biological Cybernetics*, **24** (1976), 237–240.
[24] L. Sacerdote and R. Sirovich, Multimodality of the interspike interval distribution in a simple jump-diffusion model, *Sci. Math. Jpn.*, **58** (2003), 307–322.
[25] J. P. Segundo, J. F. Vibert, K. Pakdaman, M. Stiber and O. Diez-Martinez, Noise and the neurosciences: A long history, a recent revival and some theory, *Origins: Brain and Self Organization*, (1994), 299–331.
[26] T. Shimokawa, K. Pakdaman and S. Sato, Time-scale matching in the response of a leaky integrate-and-fire neuron model to periodic stimulus with additive noise, *Phys. Rev. E*, **59** (1999), 3427–3443.
[27] H. C. Tuckwell, *Introduction to Theoretical Neurobiology: Volume 2, Nonlinear and Stochastic Theories*, Cambridge University Press, 2005.
[28] C. Van Vreeswijk, L. F. Abbott and G. B. Ermentrout, When inhibition not excitation synchronizes neural firing, *Journal of Computational Neuroscience*, **1** (1994), 313–321.
[29] F. Wan and H. C. Tuckwell, Neuronal firing and input variability, *J. Theor. Neurobiol.*, **1** (1982), 197–218.
[30] K. Wiesenfeld and F. Moss, Stochastic resonance and the benefits of noise: From ice ages to crayfish and squids, *Nature*, **373** (1995), 33–36.
[31] F. Wörgötter, E. Nelle, B. Li and K. Funke, The influence of corticofugal feedback on the temporal structure of visual responses of cat thalamic relay cells, *J. Physiol.*, **509** (1998), 797–815.

Received October 23, 2012; Accepted May 22, 2013.

E-mail address: roberta.sirovich@unito.it
E-mail address: laura.sacerdote@unito.it
E-mail address: avilla@neuroheuristic.org